



# OPEN Maturation of human induced pluripotent stem cell-derived cardiomyocytes promoted by Brachyury priming

Parisa K. Kargaran<sup>1,2,3,12</sup>, Armin Garmany<sup>2,4,5,6,12</sup>, Ramin Garmany<sup>5,6,7,8</sup>,  
Marissa J. Stutzman<sup>7</sup>, Maryam Sadeghian<sup>6,9</sup>, Michael J. Ackerman<sup>7,8</sup>,  
Carmen M. Perez-Terzic<sup>10</sup>, Andre Terzic<sup>1,2,4,8,11</sup> & Atta Behfar<sup>1,2,3,8</sup>✉

Cardiac differentiation of human induced pluripotent stem cells is readily achievable, yet derivation of mature cardiomyocytes has been a recognized limitation. Here, a mesoderm priming approach was engineered to boost the maturation of cardiomyocyte progeny derived from pluripotent stem cells under standard cardiac differentiation conditions. Functional and structural hallmarks of maturity were assessed through multiparametric evaluation of cardiomyocytes derived from induced pluripotent stem cells following transfection of the mesoderm transcription factor Brachyury prior to initiation of lineage differentiation. Transfection with Brachyury resulted in earlier induction of a cardiopoietic state as hallmarked by early upregulation of the cardiac-specific transcription factors NKX2.5, GATA4, TBX20. Enhanced sarcomere maturity following Brachyury conditioning was documented by an increase in the proportion of cells expressing the ventricular isoform of myosin light chain and an increase in sarcomere length. Mesoderm primed cells displayed increased reliance on mitochondrial respiration as determined by increased mitochondrial size and a greater basal oxygen consumption rate. Further, Brachyury priming drove maturation of calcium handling enabling transfected cells to maintain calcium transient morphology at higher external field stimulation rates and augmented both calcium release and sequestration kinetics. In addition, transfected cells displayed a more mature action potential morphology with increased depolarization and repolarization kinetics. Derived cells transfected with Brachyury demonstrated increased toxicity response to doxorubicin as determined by a compromise in calcium transient morphology. Thus, Brachyury pre-treatment here achieved a streamlined strategy to promote maturity of human pluripotent stem cell-derived cardiomyocytes establishing a generalizable platform ready for deployment.

Nuclear reprogramming of somatic cells with stemness factors has transformed the biomedical landscape, enabling to bioengineer pluripotent autologous stem cells<sup>1</sup>. Translation of pluripotent stem cells for cardiovascular applications has been facilitated through adoption of cardiogenic-lineage engagement protocols<sup>2–5</sup>. To this end, differentiation of embryoid bodies into mesodermal and subsequent cardiac lineages has provided the blueprint for the discovery of mesodermogenic and cardiogenic cues<sup>6–8</sup>. Early mesodermal and cardiac progenitor transcription factors were found to guide cell fate<sup>9–11</sup>. Identifying growth factors necessary for execution of cardiogenesis led to the development of directed differentiation protocols<sup>11,12</sup> that leverage the temporal dependence of mesoderm specification and cardiac differentiation on Wnt/ $\beta$ -catenin signaling<sup>13</sup>. Biphasic Wnt-dependent modulation encompasses initial activation of Wnt signaling to promote mesoderm

<sup>1</sup>Department of Cardiovascular Medicine, Mayo Clinic, Rochester, MN, USA. <sup>2</sup>Center for Regenerative Biotherapeutics, Mayo Clinic, Rochester, MN, USA. <sup>3</sup>Van Cleve Cardiac Regenerative Medicine Program, Mayo Clinic, Rochester, MN, USA. <sup>4</sup>Marriott Heart Disease Research Program, Mayo Clinic, Rochester, MN, USA. <sup>5</sup>Mayo Clinic Alix School of Medicine, Mayo Clinic, Rochester, MN, USA. <sup>6</sup>Mayo Clinic Graduate School of Biomedical Sciences, Mayo Clinic, Rochester, MN, USA. <sup>7</sup>Windland Smith Rice Sudden Death Genomics Laboratory, Windland Smith Rice Genetic Heart Rhythm Clinic, Mayo Clinic, Rochester, MN, USA. <sup>8</sup>Department of Molecular Pharmacology & Experimental Therapeutics, Mayo Clinic, Rochester, MN, USA. <sup>9</sup>Department of Physiology and Biomedical Engineering, Mayo Clinic, Rochester, MN, USA. <sup>10</sup>Department of Physical Medicine and Rehabilitation, Mayo Clinic, Rochester, MN, USA. <sup>11</sup>Department of Medical Genetics, Mayo Clinic, Rochester, MN, USA. <sup>12</sup>Parisa K. Kargaran and Armin Garmany are contributed equally. ✉email: behfar.atta@mayo.edu

induction, followed by subsequent Wnt inhibition to prompt cardiac lineage specification and differentiation<sup>14,15</sup>. Modulation of Wnt in monolayer cultures of engineered induced pluripotent stem (iPS) cell allows for the production of cardiomyocytes at scale for regenerative applications<sup>16</sup>, disease modeling<sup>17,18</sup> and drug toxicity screening<sup>19</sup>. However, a recognized limitation of traditional differentiation protocols of particular relevance for disease modeling and drug toxicity screening is a limited aptitude in securing cellular maturation hindering the faithful recapitulation of a genuine adult cardiomyocyte phenotype<sup>20</sup>.

Despite advances in cardiac differentiation protocols, derived progeny exhibit features of immaturity across structural, metabolic, and electrophysiological metrics<sup>20</sup>. Structurally, iPS cell-derived cardiomyocytes exhibit undeveloped structure characterized by shorter sarcomeres with expression of immature sarcomeric protein isoforms<sup>20</sup>. Similarly, electrophysiological immaturity in iPS cell-derived cardiomyocytes is exemplified by reduced action potential upstroke velocity due, in part, to low expression of sodium channels<sup>20,21</sup>. Commonly iPS cell-derived cardiomyocytes are handicapped by inherent deficits in calcium handling associated with abnormal calcium release and sequestration kinetics<sup>22</sup>. Metabolically, immature derived cardiomyocytes exhibit compromised reliance on oxidative phosphorylation and fatty acid beta-oxidation<sup>20</sup>. These aberrant properties may distort the responsiveness cardiomyocyte progeny, including deficits in detecting drug toxicity<sup>16</sup>.

Various strategies have been investigated to enhance the maturity of iPS cell-derived cardiomyocytes<sup>16</sup>. In particular, three-dimensional (3D) culture has been found to promote maturation across structural, metabolic, and electrophysiological hallmarks<sup>23</sup>. Yet complex 3D cultures remain less standardized than traditional two-dimensional (2D) monolayer cultures, requiring advanced training and imposing greater cost<sup>24</sup>. The present study therefore aimed to develop a maturation strategy deployable within monolayer culture and integrated into a standard differentiation protocol, enabling broad applicability and adoption.

Transcriptomic assessment of cells in 3D culture has revealed that mesoderm induction prior to the onset of directed differentiation is seen in cells destined for mature phenotypes<sup>25</sup>. Brachyury (T), a mesoderm factor was previously found sufficient to engender a cardiopoietic state in adult stem cells, highlighting the feasibility of T transfection for stem cell engineering<sup>26</sup>. Hence<sup>27</sup>, early mesoderm was introduced via transfection with T prior to a well-standardized 2D monolayer cardiac differentiation protocol to drive cardiomyocyte maturity.

## Results

### Brachyury transfection with Wnt modulation promotes cardiac differentiation

Whether transfection of T influences differentiation of human iPS cells, under standard biphasic Wnt modulation, was investigated by comparing beating area of cells exposed to standard differentiation (CHIR), T transfection plus standard differentiation (T+CHIR), or T transfection alone (T). Cells with and without T transfection followed by GiWi differentiation had a similar percentage of beating area 20 days after transfection (Fig. 1A;  $81 \pm 8\%$  vs  $79 \pm 8\%$ , respectively;  $p=0.57$ ). Cells transfected with T but not exposed to biphasic Wnt modulation exhibited hindered differentiation as shown by low average ( $47 \pm 19\%$ ) beating area compared to both T transfected ( $p<0.01$ ) and untransfected ( $p<0.01$ ) differentiated cells (Fig. 1A). Within 5 days, beating area in both T transfected and untransfected cells increased to  $87 \pm 3\%$  and  $88 \pm 1\%$  respectively ( $p=0.57$ ) but remained at  $48 \pm 10\%$  in cells transfected with T but without GiWi differentiation (Fig. 1A). T alone was found insufficient to induce beating areas (Fig. 1A). Thereby, T transfection along with biphasic Wnt modulation provides optimal differentiation, and was hereafter utilized.

### Brachyury transfection upregulates cardiac transcription factors

Expression of cardiac transcription factors in T primed cells was compared to untransfected cells at the corresponding day of standard cardiac differentiation to assess the impact on cardiac lineage specification. T fostered mesoderm induction of transfected iPS cells, provoking a  $6065 \pm 4815$ -fold increase in T mRNA 1 day after lipofectamine-mediated transfection compared to untransfected cells (Fig. 1B; FDR < 0.001). T expression remained  $61 \pm 34$ -fold higher 72 h after transfection compared to standard differentiation (Fig. 1B; FDR < 0.001). Activation of Wnt signaling with CHIR resulted in  $355 \pm 90$ -fold (FDR < 0.001) and  $259 \pm 105$ -fold (FDR < 0.01) higher Brachyury expression in transfected compared to untransfected cells one day and two days after Wnt activation, respectively (Fig. 1B). Inhibition of Wnt signaling with IWP-2 to promote cardiac differentiation prompted a steeper reduction in T levels in untransfected cells resulting in  $738 \pm 248$ -fold higher expression in transfected cells 48 h after cardiac specification (Fig. 1B; FDR < 0.001). Sustained upregulation of T expression in transfected compared to untransfected cells was manifested with a  $46 \pm$  eightfold increase of mRNA at 14 days after transfection (Fig. 1B; FDR < 0.01).

Transfection with T prompted a modest rise in the cardiac transcription factors NKX2.5 (Fig. 1C;  $3 \pm 0.8$ -fold; FDR < 0.05), GATA4 (Fig. 1D;  $6 \pm$  onefold; FDR < 0.01), TBX20 (Fig. 1E;  $4 \pm 0.3$ -fold; FDR < 0.01) within 24 h. In parallel, a minor reduction of relative MEF2C expression in transfected cells was observed (Fig. 1F;  $0.7 \pm 0.1$ -fold; FDR < 0.05). Following, activation of Wnt signaling, cells transfected with T exhibited bolstered upregulation of NKX2.5 (Fig. 1C;  $29 \pm$  sevenfold; FDR < 0.001), GATA4 (Fig. 1D;  $31 \pm$  sixfold; FDR < 0.01), TBX20 (Fig. 1E;  $26 \pm$  fivefold; FDR < 0.001) after 24 h compared to untransfected cells. MEF2C expression was comparable between transfected and untransfected cells 24 h after Wnt activation (Fig. 1F; FDR = 0.1) but was  $2 \pm 0.04$ -fold higher in transfected cells after 48 h (Fig. 1F; FDR < 0.05). Cardiac specification imposed by inhibition of Wnt signaling further segregated the transcription factor expression profile. Namely a  $6 \pm 0.6$ -fold expression of NKX2.5 (Fig. 1C; FDR < 0.01),  $41 \pm$  fivefold increase of GATA4 (Fig. 1D; FDR < 0.01),  $46 \pm$  twelve fold increase in TBX20 (Fig. 1E; FDR < 0.001), and  $3 \pm 0.3$ -fold increase of MEF2C (Fig. 1F; FDR < 0.01) were observed 48 h after cardiac specification.

As differentiation progressed, NKX2.5 expression remained higher in transfected cells even at 13 days after transfection (Fig. 1C;  $11 \pm 0.8$ -fold; FDR < 0.001). At 14 days post transfection, TBX20 expression (Fig. 1E;  $6 \pm 0.7$ -fold change; FDR < 0.001) also remained upregulated in mesoderm potentiated cells. Expression of the

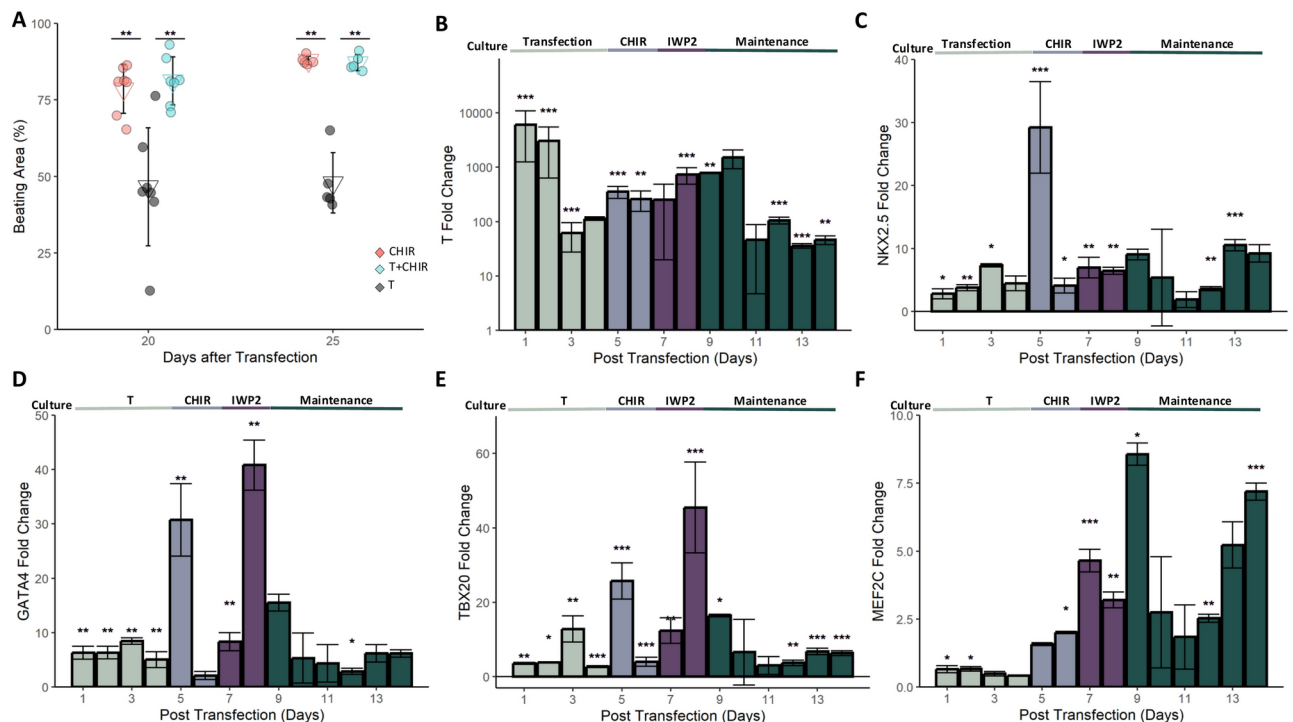


**Fig. 1.** T transfection prior to standard cardiac differentiation instills sustained upregulation of cardiac transcription factors. **(A)** Induced pluripotent stem cells undergoing standard differentiation with and without T transfection exhibited similar beating areas. Wnt modulation was required for maximal beating area. T+CHIR denotes cells transfected with T that undergo biphasic Wnt modulation for cardiac differentiation. CHIR denotes untransfected cells that are differentiated with Wnt modulation. T indicates cells transfected with T but not exposed to standard differentiation. **(B)** Brachyury expression in T transfected cells was increased within 24 h of transfection and remained upregulated compared to untransfected cells. **(C)** Maximum upregulation of NKX2.5 in transfected cells versus untransfected cells was observed upon mesoderm induction with CHIR. **(D)** GATA4 expression showed an increase in transfected cells during culture with CHIR and peaked with subsequent Wnt inhibition. **(E)** TBX20 expression was bolstered in mesoderm potentiated cells. **(F)** MEF2C expression in T transfected cells was observed following upregulation of other cardiac transcription factors. Error bars represent standard deviation. **(B–F)** Fold changes compare T transfected cells to untransfected cells at each corresponding day of differentiation. \* $p < 0.05$ , \*\* $p < 0.01$ , \*\*\* $p < 0.001$ .

late cardiac transcription factor MEF2C remained similar between transfected and untransfected cells until after cardiac specification engagement when robust MEF2C upregulation was observed starting at post-transfection day 7 (Fig. 1F;  $5 \pm 0.4$ -fold; FDR  $< 0.001$ ). MEF2C expression peaked at 72 h after cardiac specification (Fig. 1F;  $9 \pm 0.4$ -fold; FDR  $< 0.01$ ) and remained elevated 13 days after transfection (Fig. 1F;  $5 \pm 0.9$ -fold; FDR  $< 0.001$ ). Thus, compared to untransfected iPS cells, transfection of T sensitizes cells to lineage specification cues, resulting in augmented sustained upregulation of cardiac transcription factors.

### Mesoderm potentiation increases differentiation efficiency

The influence of T, a mesoderm inducer, on cardiac differentiation and lineage specification were investigated by assessing the proportion of derived progeny expressing the cardiac marker, cardiac Troponin T (cTnT), the atrial lineage marker, myosin light chain 2A (MLC2A), and the ventricular lineage marker myosin light chain 2 V (MLC2V) (Fig. 2A). T transfection increased the proportion of derived cells expressing troponin from  $77 \pm 0.04\%$  to  $90 \pm 0.03\%$  (Fig. 2B;  $p < 0.05$ ), MLC2A expressing cells from  $12 \pm 0.03\%$  to  $27 \pm 0.05\%$  (Fig. 2B;  $p < 0.05$ ), and MLC2V positivity from  $54 \pm 0.04\%$  to  $82 \pm 0.03\%$  (Fig. 2B;  $p < 0.0001$ ). Thus, T transfection had a particularly pronounced impact on ventricular lineage specification, increasing positivity by  $\sim 30\%$  (Fig. 2C).

### Brachyury transfection augments structural maturity and mitochondrial energy metabolism

At the ultrastructural level, maturity of iPS cell-derived cardiomyocytes was probed using electron microscopy to determine sarcomere length (Fig. 3A). T transfection increased the average sarcomere length of iPS cell-derived cardiomyocytes from  $1.56 \pm 0.03 \mu\text{m}$  to  $1.67 \pm 0.03 \mu\text{m}$  (Fig. 3B;  $p < 0.05$ ). Mitochondrial size in transfected and untransfected cells was quantified using transmission electron micrographs (Fig. 3C). Individual mitochondrial kernel density area estimates (Fig. 3D;  $p < 0.001$ ) revealed a greater mitochondrial size in T transfected cells ( $n = 1761$  mitochondria) than untransfected cells ( $n = 1287$  mitochondria) with an average mitochondrial size of  $0.17 \pm 0.01 \mu\text{m}^2$  and  $0.14 \pm 0.01 \mu\text{m}^2$  per field for transfected and untransfected cells, respectively (Fig. 3E;  $p < 0.05$ ).

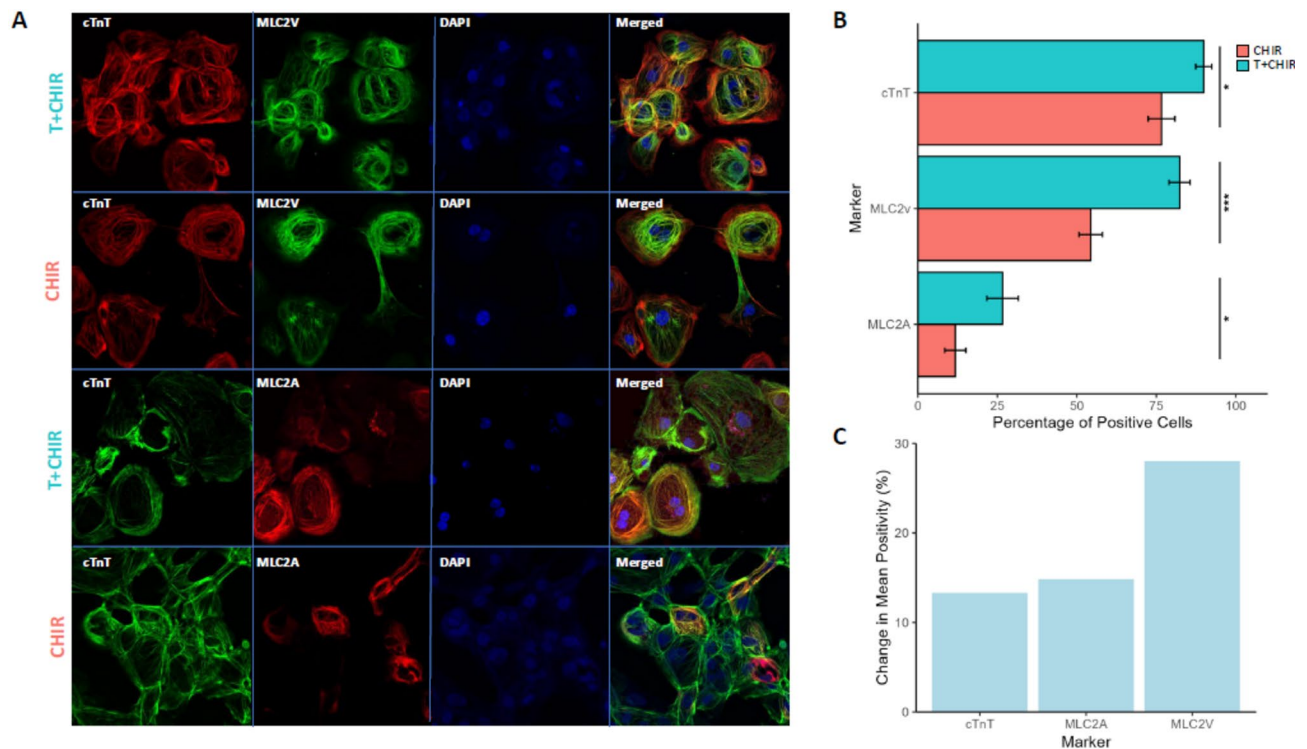


**Fig. 2.** Mesoderm potentiation increases differentiation efficiency. **(A)** Differentiated iPS were labeled for cardiac troponin T (cTnT), myosin light chain 2v (MLC2V), and myosin light chain 2a (MLC2A). **(B)** MLC2V, MLC2A, and cTnT positivity were all increased following T transfection. **(C)** MLC2V was positivity preferentially increased with mesoderm priming before differentiation. \* $p < 0.05$ , \*\*\* $p < 0.001$  T + CHIR denotes cells transfected with T that undergo biphasic Wnt modulation for cardiac differentiation. CHIR denotes untransfected cells that are differentiated with Wnt modulation.

Moreover, T transfected cells tended to have a higher average mitochondrial DNA copy number, although this difference was not statistically significant (Fig. 3F;  $p = 0.28$ ). The reliance of differentiated cardiomyocytes on mitochondrial respiration was estimated by measuring oxygen consumption rates (Fig. 3G). As early as 35 days after differentiation, Brachyury transfection increased basal reliance on oxidative phosphorylation as manifested by an increase from  $2.04 \pm 0.09$  pmol  $O_2$ /min/1000 in untransfected cells to  $2.69 \pm 0.21$  pmol  $O_2$ /min/1000 in T transfected counterparts (Fig. 3H; FDR  $< 0.05$ ). Maximal respiration (FDR = 0.88) and spare respiratory capacity (FDR = 0.37) remained similar across cell cohorts (Fig. 3H). Thus, T transfection enhances sarcomere maturity, mitochondrial size, and basal reliance on oxidative phosphorylation.

### Brachyury instills calcium handling resilience

Calcium handling of iPS cell-derived cardiomyocytes was interrogated under external field stimulation with the calcium sensitive fluorophore Fluo-4 (Fig. 4A). Derived cardiomyocytes, 15 days after differentiation, exhibited shortening of calcium transients in response to increased pacing frequency (Fig. 4B). However, as pacing reached a frequency of 2 Hz, only T transfected cells maintained their calcium transient morphology (Fig. 4B and inset). Specifically, at a pacing of 0.5 Hz, the transient width<sub>70</sub> (reflecting the time needed to reach a 70% return to baseline), for untransfected cells was  $1293 \pm 0.5$  ms and was reduced to  $1260 \pm 0.6$  ms in T transfected cells (Fig. 4C; FDR  $< 0.05$ ). Transfected cells also exhibited greater transient amplitudes (Fig. 4D; FDR  $< 0.001$ ) and larger calcium transient integrals (Fig. 4E; FDR  $< 0.001$ ), reflective of an augmented overall calcium transportation capacity. At this external field stimulation rate, upstroke transient kinetics (Fig. 4F; FDR = 0.06), namely maximum slope ( $V_{max}$ ) and calcium sequestration/efflux kinetics (Fig. 4G; FDR = 0.24), assessed as time constant of decay ( $\tau$ ) were similar regardless of transfection status. Both T transfected and untransfected cells exhibited a shortening of transient width<sub>70</sub> at a field stimulation of 1 Hz, yet T transfected cells demonstrated significantly shorter transients (Fig. 4C; FDR  $< 0.01$ ). In fact, transfected cells displayed greater transient amplitudes (Fig. 4D; FDR  $< 0.001$ ) and peak areas (Fig. 4E; FDR  $< 0.001$ ) along with an accentuated  $V_{max}$  (Fig. 4F; FDR  $< 0.001$ ) and reduced  $\tau$  (Fig. 4G; FDR  $< 0.001$ ). Raising field stimulation to 1.5 Hz, deformed calcium transients of untransfected cells, with an excessive reduction of width<sub>70</sub> (Fig. 4C; FDR  $< 0.01$ ) and a reduced transient amplitude (Fig. 4D; FDR  $< 0.001$ ) and integral (Fig. 4E; FDR  $< 0.001$ ). These changes collectively point to compromised calcium cycling contrasting with the more resilient T transfected cells. In fact, at 1.5 Hz transfected cells exhibited preserved kinetic responses in both  $V_{max}$  (Fig. 4F; FDR  $< 0.001$ ) and  $\tau$  (Fig. 4G; FDR  $< 0.001$ ). Thus, T transfection instilled improved calcium handling aptitude in the setting of imposed workload.



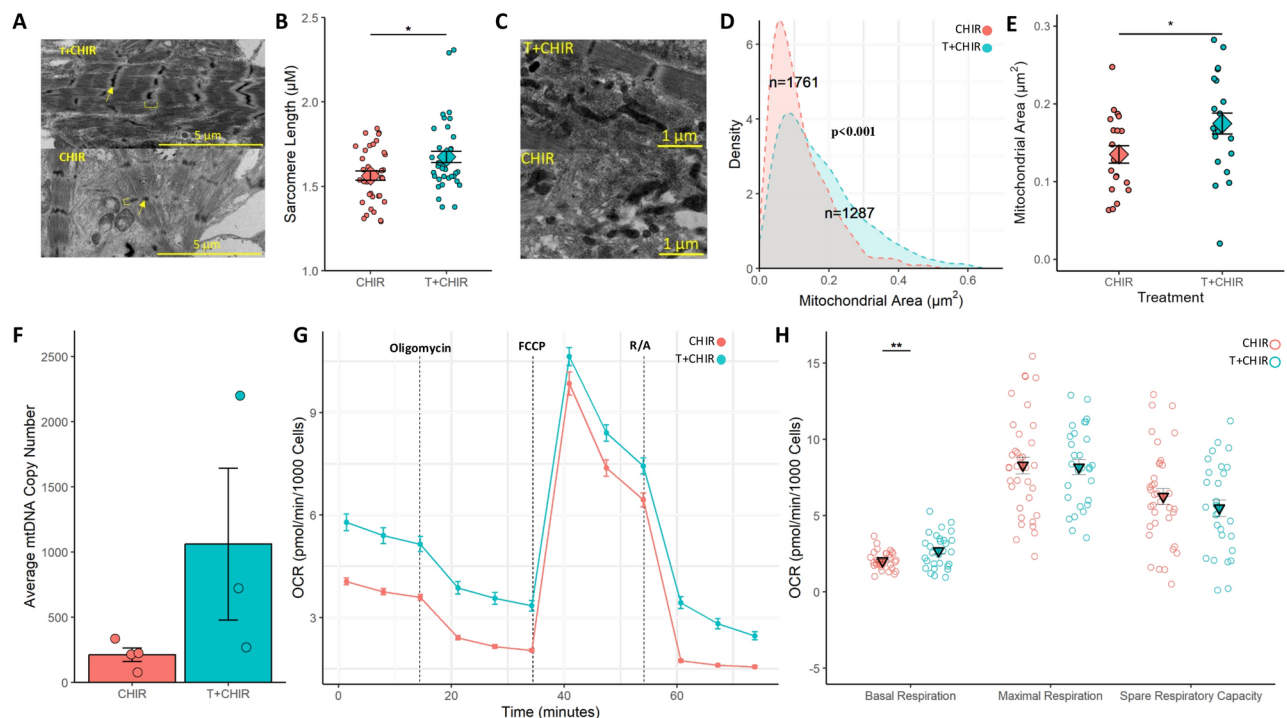


**Fig. 3.** Priming with Brachyury promotes structural and metabolic maturity. (A) Transmission electron microscopy enabled visualization of I bands (brackets) and Z-lines (arrows). (B) Transfection endowed increased sarcomere length. (C) Mitochondrial area was quantified in transfected and untransfected cells. (D) Kernel density estimates of mitochondrial area reveal a distinct larger distribution in transfected cells compared to untransfected cells. (E) Average mitochondrial area per field was augmented in transfected cells. (F) Average mitochondrial DNA copy number tended to be higher in transfected cells but exhibited high variability. (G) A seahorse assay allowed interrogation of shifts in metabolic reliance. R/A denotes rotenone and antimycin and FCCP indicates carbonyl cyanide 4-(trifluoromethoxy) phenylhydrazone. (H) T transfection promoted an increase in basal respiration oxygen consumption 35 d after differentiation. \* $p < 0.05$ , \*\* $p < 0.01$ . T + CHIR denotes cells transfected with T that undergo biphasic Wnt modulation for cardiac differentiation. CHIR denotes untransfected cells that are differentiated with Wnt modulation.

### T Transfection induction endows mature action potential features

Action potentials of T transfected (Fig. 5A) and untransfected cells (Fig. 5B) were assessed under 2 Hz external field stimulation via the voltage sensitive dye FluoVolt following 35 days of differentiation. Distinct action potential presentation was observed in cells primed with T transfection (Fig. 5C). T transfected cells displayed an average action potential duration 70 (APD<sub>70</sub>), reflecting the time needed to reach a 70% return to resting potential, of  $228 \pm 0.4$  ms contrasting the  $208 \pm 2$  ms long action potential in untransfected cells (Fig. 5D, FDR<0.001). The maximum slope of depolarization was augmented in transfected cells ( $4.2 \pm 0.03$  AU/s vs  $2.7 \pm 0.03$  AU/s; Fig. 5E; FDR<0.001) while the minimum slope of repolarization was steeper ( $-2.3 \pm 0.02$  AU/s vs  $-1.4 \pm 0.01$  AU/s; Fig. 5F; FDR<0.001) and the decay constant, tau, reduced (Fig. 5G; FDR<0.001). Thus, under equivalent imposed pacing, transfected cells display advanced action potential kinetics.

### T Transfection inoculates augmented doxorubicin sensitivity

At 35 days of differentiation, T transfected cells loaded with Fluo-4 and paced at 1 Hz (Fig. 6A) had a greater transient amplitude ( $1.4 \pm 0.04$  AU vs  $1.1 \pm 0.01$  AU; Fig. 6B; FDR<0.001), a shorter transient width<sub>70</sub> ( $562 \pm 16$  ms vs  $678 \pm 12$  AU; Fig. 6C; FDR<0.001), an increased maximum upstroke velocity ( $4.07 \pm 0.6$  AU/s vs  $0.6 \pm 0.05$ ; Fig. 6D; FDR<0.001) and an augmented minimum relaxation velocity ( $-1.59 \pm 0.2$  vs  $-0.28 \pm 0.01$ ; Fig. 6E; FDR<0.001) when compared to untransfected counterparts. To evaluate whether T transfected cells have acquired a genuine responsiveness to a conventional cardiotoxic challenge, cells were exposed to 1  $\mu\text{M}$  doxorubicin for over a period of ~24 h (Fig. 6A). In response to doxorubicin challenge, untransfected cells showed a  $<1 \pm 0.7\%$  increase in calcium transient width<sub>70</sub> while transfected cells displayed a  $24 \pm 0.7\%$  change (Fig. 6F; FDR<0.001). In addition, transfected cells displayed a  $21 \pm 0.5\%$  reduction in transient amplitude compared to a  $6 \pm 0.6\%$  increase in untransfected cells (Fig. 6G; FDR<0.001). Furthermore, transfected cells showed a greater compromise in calcium kinetics documented with a reduction in maximum upstroke velocity ( $-64 \pm 0.9\%$  vs  $65 \pm 4\%$ ; Fig. 6H; FDR<0.001). Transfected and untransfected cells showed similar decline in cell viability with increasing doxorubicin dose (Fig. 6I;  $p > 0.05$ ). Thus, with T transfection, iPS cell-derived cardiomyocytes exhibit salient features of doxorubicin toxicity.

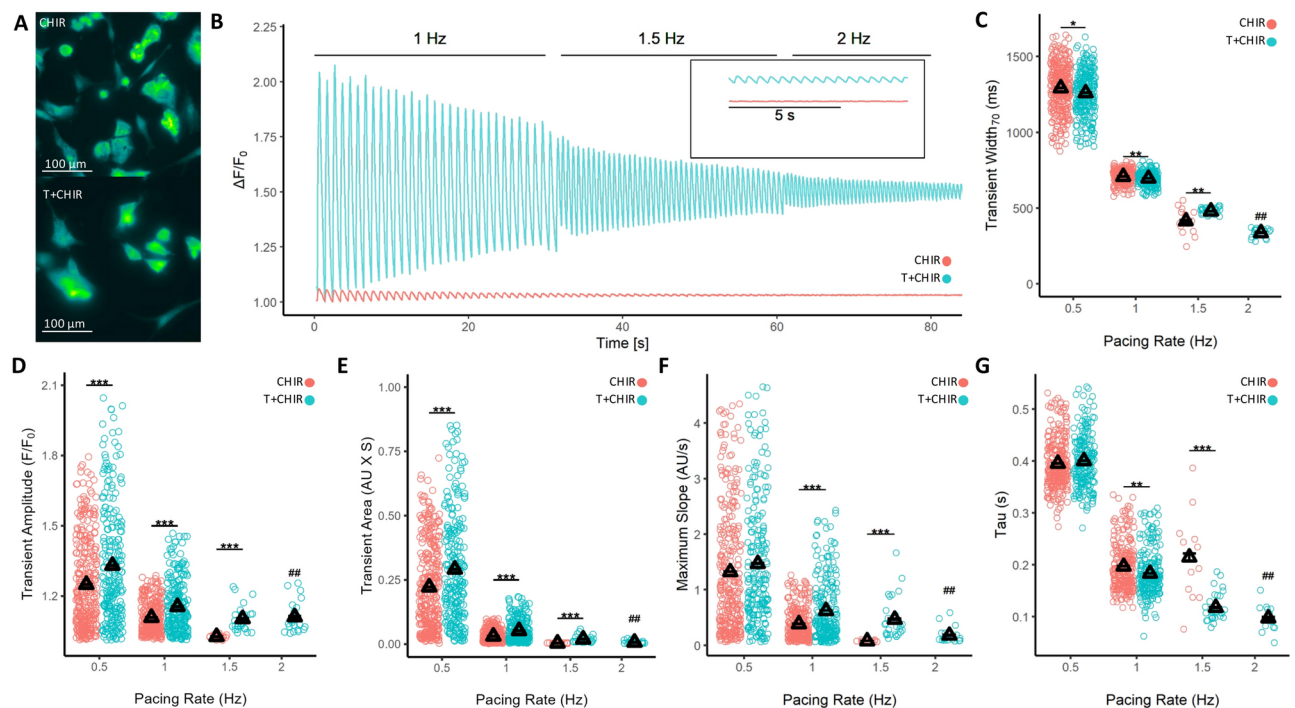


**Fig. 4.** Mesoderm prepotentiation imparts calcium handling resilience. (A) Fluo-4 staining of iPS cardiomyocytes at 15 d of differentiation allowed assessment of calcium handling. (B) Cells were paced with an external field stimulation of 0.5 Hz to 2 Hz. T primed cells were able to maintain calcium transient morphology with up to 2 Hz external field stimulation whereas untransfected cells exhibited compromised calcium handling (B inset). (C) T transfected cells were able to appropriately shorten transient width<sub>70</sub>, reflecting the time needed to reach a 70% return to baseline, with increasing external field stimulation rate. Mesoderm induction before differentiation promoted greater calcium handling as shown by increased transient amplitudes (D) and transient area (E). T transfected cells exhibited faster kinetics as shown by a greater maximum upstroke velocity (F) and lower decay constant, tau (G). T + CHIR denotes cells transfected with T that undergo biphasic Wnt modulation for cardiac differentiation. CHIR denotes untransfected cells that are differentiated with Wnt modulation. \* $p < 0.05$ , \*\* $p < 0.01$ , \*\*\* $p < 0.001$ , ## no CHIR cells were able to maintain transient morphology with 2 Hz external field stimulation.

## Discussion

The present study establishes a single transcription factor-based maturation protocol that generates mature cardiomyocytes under standard differentiation of human iPS cell monolayers. To date, protocols to achieve desired maturity have traditionally relied on complex or prolonged culture<sup>20,28–34</sup>, adding cost and intricacy while compromising standardization and adoptability<sup>24</sup>. To augment the maturity of the iPS cell-derived cardiomyocyte pool, we here imposed mesoderm pre-priming by dialing-up Brachyury expression, thereby escaping the need for 3D or extended culture<sup>15</sup>. Brachyury was selected among mesoderm factors given its efficacy in single-factor cell engineering<sup>26</sup> and in driving mesoderm specification in pluripotent stem cells<sup>27</sup>. Early induction of a mesoderm state during differentiation, as achieved here, promoted structural and functional maturity of iPS cell-derived cardiomyocytes that acquired a heightened cardiotoxicity response. This study thus provides a readily deployable bioengineered platform that yields human iPS cell-derived cardiomyocyte progeny with improved phenotypic fidelity.

## Cardiogenic guidance

Here transfection with T prompted induction of mesoderm before turning on Wnt signaling as hallmarked by upregulation of Brachyury within differentiating iPS cells. Such early mesoderm induction has been associated with an acceleration in the maturation of cellular progeny<sup>25</sup>. As observed here, mesoderm preinduction was triggered by spiking Brachyury expression which remained elevated throughout differentiation. Introduction of T alone has been pinpointed to be sufficient in engineering a cardiopoietic state in adult stem cells characterized by nuclear upregulation of cardiac progenitor transcription factors, namely NKX2.5 and GATA4<sup>35</sup>. T alone however was unable to promote robust sarcomerogenesis, highlighting its purported role as an inducer of the cardiopoietic state rather than a direct promotor of sarcomerogenesis<sup>35</sup>. These findings are inline in with findings showing induction of a cardiopoietic state in adult stem cells following T transfection<sup>26</sup>. This directed early transition to a cardiac progenitor state was further boosted with Wnt activation through GSK-3 inhibition, a known promotor of mesoderm guidance<sup>36</sup>. This transition into a cardiac lineage prior to external Wnt inhibition has been attributed to autocrine/paracrine-mediated inhibition of Wnt imposed by nearby mesoderm

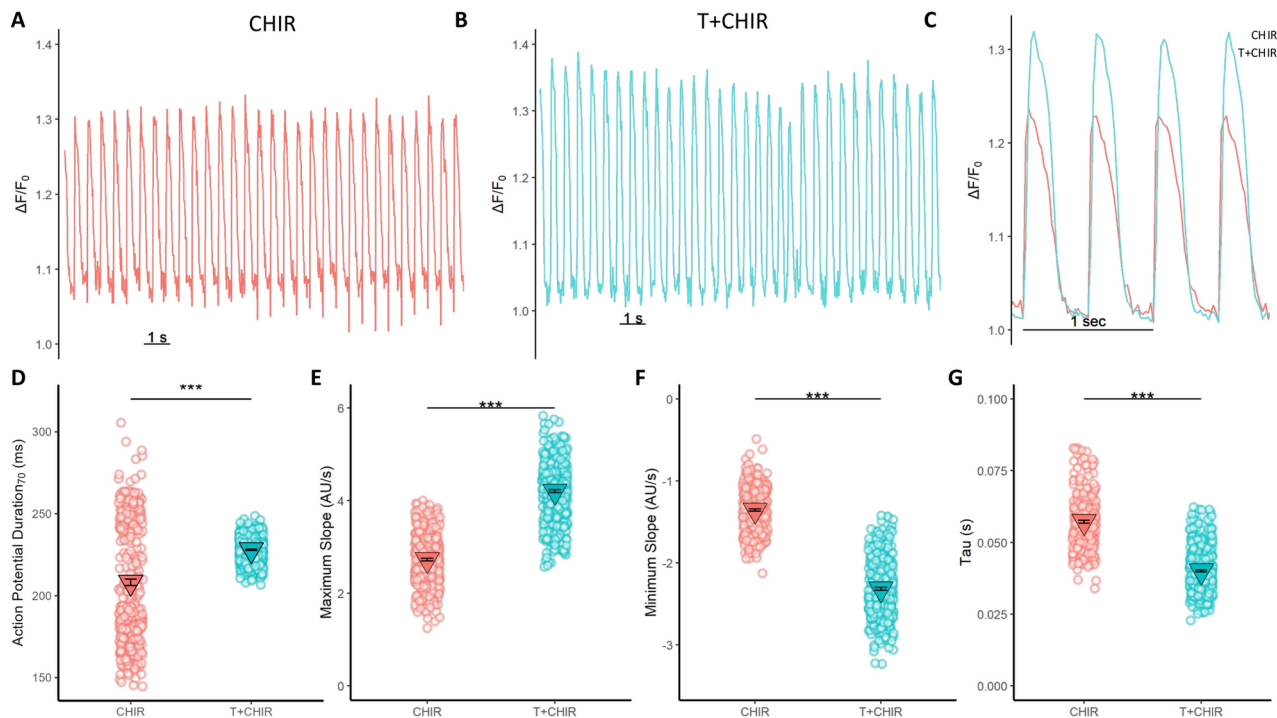


**Fig. 5.** T transfected cells display more mature action potential morphologies. Untransfected (A) and T transfected (B) cells were stained with FluoVolt for assessing action potential morphology with 2 Hz external field stimulation. (C) Superimposed averaged action potential traces reveal distinct action potential shape between culture conditions. Action potential duration 70 is increased in T transfected cells (D) with an increase in maximum upstroke velocity (E) and enhanced minimum repolarization slope (F) and a lower decay constant, tau (G). T + CHIR denotes cells transfected with T that undergo biphasic Wnt modulation for cardiac differentiation. CHIR denotes untransfected cells that are differentiated with Wnt modulation.

committed cells<sup>37</sup>. In line with normal orchestration of cardiac transcription factors during cardiogenesis, a delayed upregulation of MEF2C, a transcription factor required for sarcomere expression, was observed<sup>38,39</sup>. Collectively, the applied protocol realizes bolstered recapitulation of the expression profile typifying cardiogenic induction.

### Sarcomeric maturation

Here sarcomere maturity was documented by tracking sarcomeric protein isoform expression and sarcomere structure. The myosin regulatory light chain 2 atrial (MLC2a) and ventricular (MLC2v) isoforms exhibit distinct expression distributions in the postnatal heart and are associated with unique molecular signatures<sup>40,41</sup>. MLC2v expression is confined to the postnatal ventricle whereas MLC2a is initially expressed in all heart chambers and becomes confined to the atria as development progresses<sup>16,42</sup>. Here, a modest increase of MLC2a expression was observed, in line with a beneficial influence on atrial phenotype maturation. However, a preferential increase in MLC2v positivity was observed suggesting increased maturity of ventricular-like cardiomyocytes as an increased MLC2v<sup>+</sup> has been associated with a greater maturity phenotype<sup>42,43</sup>. In addition, maturing cardiomyocytes exhibit a progressively increased sarcomere length<sup>23,44</sup> which was documented in the present study at the ultrastructural level following T induction. Taken together, iPS cell-derived progeny that underwent early mesoderm induction exhibited structural hallmarks of maturing cardiomyocytes.

### Metabolic reprogramming

Synchronous to structural remodeling, postnatal cardiac development is associated with a metabolic conversion characterized by increased reliance on fatty acid oxidation and mitochondrial respiration<sup>45,46</sup>. Mature iPS cell-derived cardiomyocytes show augmented oxygen consumption even under basal conditions<sup>47,48</sup>. Mesoderm potentiation here resulted in increased basal oxygen consumption, in line with a greater utilization of mitochondrial respiration. Increased reliance on mitochondrial respiration in mature cardiomyocytes has been accompanied by increased mitochondrial size<sup>49</sup>. Here, T transfected cells exhibited greater mitochondrial size and a trend towards higher mtDNA copy numbers as anticipated for maturing cardiomyocytes.

### Electrophysiological maturity

Electrophysiological maturity of cardiomyocytes is observed in calcium handling and action potential morphology<sup>20</sup>. Low-throughput approaches including patch clamp electrophysiology remain the gold-standard for assessing ion channel activity and properties<sup>50,51</sup>. High-throughput single-cell resolution offered by optical

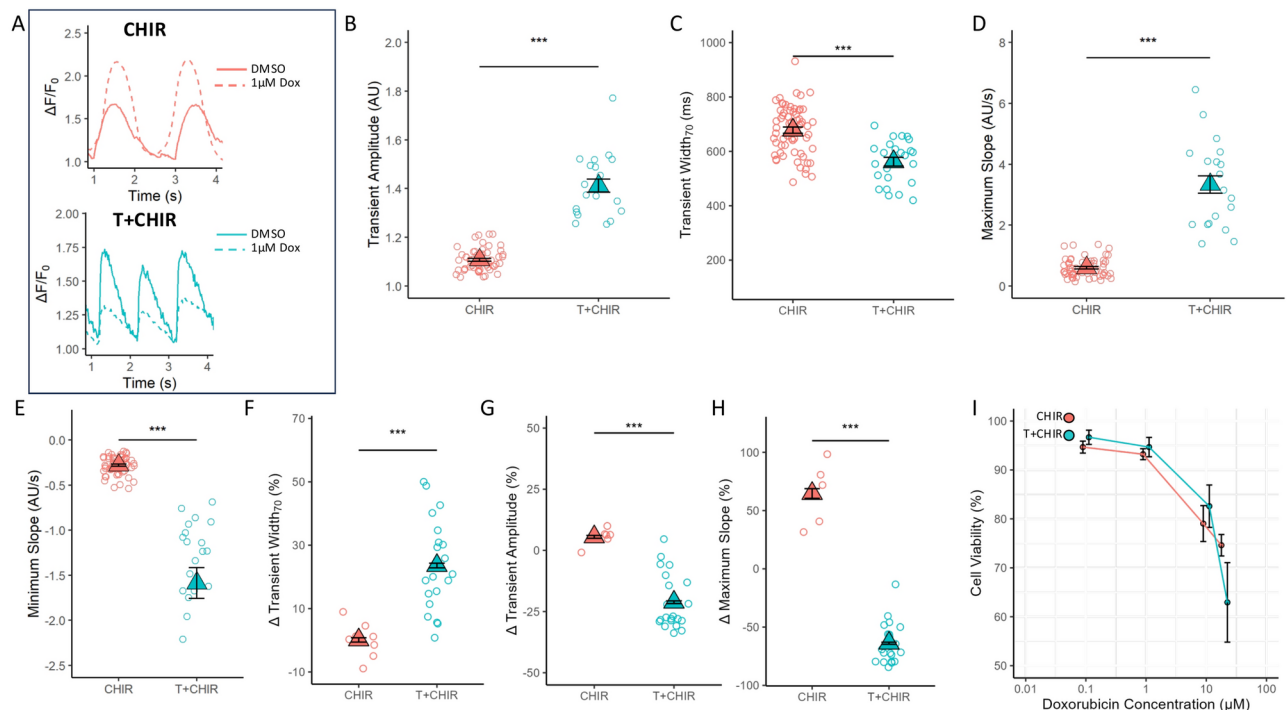


**Fig. 6.** Enhanced toxicity readouts were observed in T transfected cells. (A) Calcium transients were optically mapped using Fluo-4 staining of cells in the presence or absence of 1  $\mu$ M doxorubicin in DMSO with an external field stimulation of 1 Hz 35 d after differentiation. T transfection led to calcium transients with greater amplitudes (B) and shorter transient duration width<sub>70</sub> (C) with concomitant augmentation of maximum transient upstroke velocity (D) and minimum transient relaxation velocity (E). Cells primed with T showed amplified response to doxorubicin manifesting as an exaggerated calcium transient width<sub>70</sub> prolongation (F), greater reduction in transient amplitude (G), and maximum slope decline (H) compared to untransfected cells. To account for differences in maturity, the percent  $\Delta$  for each parameter was calculated as the percent difference between each cell and the mean of the unexposed doxorubicin cells for each group. (I) Propidium iodide staining showed similar dose dependent decline in cell viability with increasing doxorubicin concentration. T + CHIR denotes cells transfected with T that undergo biphasic Wnt modulation for cardiac differentiation. CHIR denotes untransfected cells that are differentiated with Wnt modulation. \* $p < 0.05$ , \*\* $p < 0.01$ , \*\*\* $p < 0.001$ .

mapping was used here in the context of inter-cell variability and density-dependent phenotypes observed with iPS cell-derived cardiomyocytes cultured as monolayers<sup>50,51</sup>. With acquired maturity, iPS cell-derived cardiomyocytes progressively increase sarcoplasmic calcium stores, expression and functionality of calcium handling proteins, and exhibit accelerated calcium transient kinetics<sup>29</sup>. As early as 15 days after initiation of differentiation, distinct calcium handling behavior was observed in T transfected versus untransfected cells. Namely, transfected cells were able to maintain appropriate calcium transient profiles even at accelerated pacing, demonstrating faster calcium kinetics and greater calcium transient amplitudes. Robust calcium handling persisted 35 days into differentiation of mesoderm-primed cells. In tandem with augmented calcium handling, evolution of electrical features is a hallmark of cardiogenic maturity<sup>52</sup>. Mature action potentials are characterized by a pronounced upstroke velocity due to a polarized resting membrane potential and greater expression of an adult sodium channel subunit isoform<sup>16</sup>, and display rate-dependent action potential shortening<sup>53</sup>. In line with acquisition of an increasingly mature electrophysiological ensemble, T transfected cells showed an augmented maximum upstroke velocity and accelerated relaxation kinetics and were thus fit to shorten on demand their action potential duration, underscoring electrophysiological remodeling.

### Amplified toxicity response

Increasingly, iPS cell-derived cardiomyocytes are leveraged for disease modeling and drug toxicity applications<sup>54</sup>. Applicability of iPS cell technology mandates recapitulation of mature physiology and disease phenotypes<sup>55,56</sup>. We here documented the response of transfected cells to the cardiotoxic chemotherapy agent doxorubicin<sup>57–59</sup>, suggested to impose cardiotoxicity via mechanisms other than its therapeutic role as a topoisomerase inhibitor<sup>60</sup>, in part attributed to activation of apoptosis<sup>61,62</sup> and disruption of calcium homeostasis<sup>60</sup>. T priming sensitized iPS cell-derived cardiomyocytes towards doxorubicin toxicity, with greater doxorubicin-induced compromise in calcium handling and a reduction in calcium transient amplitude and transient prolongation, consistent with doxorubicin-induced disruption of calcium homeostasis<sup>63</sup>. Thus, T transfection amplifies the toxicity response of iPS cell-derived cardiomyocytes.



## Conclusion

We here introduce a single transcription factor approach to promote the maturity of human iPS cell-derived cardiomyocytes. Mesoderm priming, imposed by T transfection before induction of differentiation, resulted in boosting the expression of cardiogenic transcription factors resulting in enhanced structural, metabolic, and electrophysiological maturity along with more robust cardiac toxicity response. The value of this engineered platform in streamlining derivation of mature cardiomyocytes and offering a bona fide model system requires further independent validation.

## Methods

### Induced pluripotent stem cell culture

iPS cells were obtained from the Mayo Clinic Center for Regenerative Biotherapeutics Biotrust from human fibroblast biopsies under Mayo Clinic Institutional Review Board approval (IRB #22–011,716) at passage 7. At time of reprogramming, karyotype analysis and primary germ layer tissue differentiation analyses were conducted by the Mayo Clinic Center for Regenerative Biotherapeutics Biotrust to ensure quality control. Biobanked iPS cells were thawed and cultured under feeder-free conditions with mTeSR Plus media (Stem Cell Technologies, MA, USA) as previously described<sup>64</sup>.

### mRNA Transfection

iPS cells were plated in a 6-well plate at a density of 90,000/well, and transfected 72 h prior to induction of cardiomyocyte differentiation with 1.75 µg of T RNA in OptiMEM media (ThermoFisher, MA, USA) using 3 µL of Lipofectamine Stem Transfection Reagent (ThermoFisher, MA, USA), incubated for 9 min prior to cell transfection<sup>35</sup>.

### Cardiomyocyte differentiation

Pluripotent cells were differentiated using a glycogen synthase kinase 3 (GSK3) inhibitor and Wnt inhibitor (GiWi) protocol. To impose mesoderm lineage guidance, mTeSR media was exchanged for RPMI supplemented with B27 minus insulin (ThermoFisher, MA, USA) with 5 µM CHIR99021 (CHIR, Stem Cell Technologies, MA, USA). After 48 h, cells were cultured in RPMI/B27 without insulin for 12 h followed by supplementation with 5 µM IWP-2 (Stem Cell Technologies, MA, USA) for 48 h to promote cardiac lineage guidance. Following the onset of beating, cardiomyocytes were purified using lactate selection. Cells were cultured in RPMI with 500 µg/mL of human albumin (Sigma-Aldrich, MA, USA), 217 µg/mL of ascorbic acid (Sigma-Aldrich, MA, USA), and 5 mM of D-lactate (Sigma-Aldrich, MA, USA) for 7-days<sup>64</sup>. RPMI supplemented with B27 was used for cell maintenance after purification of cardiomyocytes.

### RNA Expression analysis

RNA was extracted using the RNeasy Plus Mini Kit (Qiagen, Hilden, Germany) and quantified using a NanoDrop ND-1000 spectrophotometer (ThermoFisher, MA, USA). Quantitative reverse transcription polymerase chain reaction (RT-qPCR) was conducted using the 1-step QuantiTect SYBR® Green RT-PCR Kit (Qiagen, Hilden, Germany) with the ViiA 7 Real-Time PCR System (Applied Biosystems, MA, USA). All experiments were performed in biological triplicates. Fold change was calculated using the  $2^{-\Delta\Delta CT}$  method with statistical comparisons conducted on  $\Delta CT$  values<sup>65,66</sup>. Values are reported as fold changes  $\pm$  standard deviation.

### Immunofluorescence

Cells were harvested using the STEM Cardiomyocyte Dissociation Kit (Stem Cell Technologies, MA, USA) following manufacturer's instructions and plated into Chambered Cell Culture Slides (Celltreat Scientific Products, MA, USA) for two days. Cells were washed with phosphate-buffered saline (PBS) fixed with 4% paraformaldehyde for 10 min at room temperature (RT). After three PBS washes, cells were blocked with 0.1% Triton X-100/ PBS (PBS-T)/5% goat serum for 1 h at RT. Fixed cells were incubated at 4 °C overnight in the primary antibody solution consisting of PBS-T/5% goat serum containing a 1:250 dilution of antibodies against MLC2A (ThermoFisher, MA, USA), MLC2V (ThermoFisher, MA, USA), and cTnT (Abcam, MA, USA). The following day, cells were washed three times with PBS-T/5% goat serum at RT before being incubated for 1 h in PBS-T/5% goat serum with Alexa Fluor® 488 goat anti-rabbit (ThermoFisher, MA, USA) and Alexa Fluor® 594 goat-anti-mouse (ThermoFisher, MA, USA) secondary antibodies at a dilution of 1:200. After secondary antibody incubation, cells were washed three times with PBS-T and DAPI was added to the final wash at a dilution of 1:2000. Mounting solution and coverslips were placed on slides. Images were acquired on a Zeiss LSM 780 confocal microscope. Zen Blue (v3.8.99.0000; ZEISS, Oberkochen, Germany) analysis software was used for fluorescence quantification.

### Beating area quantification

The Axiovert 40 inverted phase contrast microscope (Zeiss, Oberkochen, Germany) was used to acquire video microscopy images and Zen software (v3.8.99.0000; Zeiss, Oberkochen, Germany) was used to capture beating activity. Beating areas (%)  $\pm$  standard deviation are reported.

### Sarcomere length and mitochondrial morphometry

Cells between 20–30 days after initiation of the GiWi differentiation protocol were cultured on ACLAR embedding film for two days and fixed with Trump's fixative solution (pH 7.2) at 4 °C overnight. Fixed cells were microwave processed using a Leica EM AMW microwave processor. Following a PBS rinse cells were post-fixed in 1% osmium tetroxide, rinsed with distilled water, stained with 2% uranyl acetate, rinsed with distilled water,

dehydrated through a graded series of ethanol, further dehydrated with acetone, and infiltrated with epoxy resin via acetone. Processed samples were then embedded into either pure Spurr or Elong/Araldite resin blocks. Ultrathin (0.1  $\mu\text{m}$ ) sections were cut and mounted on 200-mesh copper grids, post-stained with lead citrate, and visualized under a JEOL JEM-1400 and/or JEM-1400 Plus transmission electron microscope (JEOL USA, MA, USA) at 80 kV. Sarcomere length, defined as the distance between z-lines, and mitochondrial area were measured using Fiji software (v2.15.)<sup>67</sup>.

### Mitochondrial DNA copy number

Cells were lysed and DNA was extracted using the QIAamp DNA Mini Kit (Qiagen, Hilden, Germany). RT-qPCR was conducted with the The Human Mitochondrial DNA (mtDNA) Monitoring Primer Set (Takara Bio USA, Inc., CA, USA) and Terra qPCR Direct TB Green Premix (Takara Bio USA, Inc., CA, USA) on a ViiA 7 Real-Time PCR System (Applied Biosystems, MA, USA) to determine mtDNA copy, estimated as the average  $2^{\Delta\text{CT}}$  for two pairs of mtDNA and nuclear DNA genes<sup>68</sup>. Experiments were performed in biological triplicates.

### Seahorse assay

A mitochondrial stress assay was conducted using the seahorse XF Cell mito stress test kit (Agilent technologies, CA, USA). Cells were plated into a XFe96 Cell Culture Microplate (Agilent Technologies, CA, USA) and maintained until reaching 80% confluency. Seahorse XF DMEM (Agilent Technologies, CA, USA) was supplemented with 10 mM glucose, 2 mM glutamine, and 1 mM pyruvate. Prior to initiation of the assay, cells were incubated in the absence of  $\text{CO}_2$  for 1 h. Mitochondrial function was evaluated following serial exposure to oligomycin (100  $\mu\text{M}$ ), carbonyl cyanide 4-(trifluoromethoxy) phenylhydrazone (FCCP; 100  $\mu\text{M}$ ) and rotenone/antimycin A (50  $\mu\text{M}$ ). Oxygen consumption rates were measured on a Xfe96 Seahorse Analyzer (Agilent Technologies, CA, USA). Parameters of mitochondrial function were calculated as per manufacturer's instructions. Namely, basal respiration was calculated as the last rate measurement before first injection—nonmitochondrial respiration rate. Maximal respiration was calculated as maximum rate after FCCP injection—nonmitochondrial respiration rate. Spare respiratory capacity was defined as maximal respiration – basal respiration. Oxygen consumption rates were normalized to cell number using the Cytation 5 cell imaging multimode reader (BioTek, VT, USA).

### Fluorescence-based live cell imaging

Thirty-five mm glass-bottom dishes (MatTek, MA, USA) were coated with Matrigel (Corning, NY, USA). Cardiac differentiated iPS cells were plated 48 h before imaging. Prior to staining, cells were washed with standard Tyrode's solution containing in mM: 130-NaCl, 5.4-KCl, 10-HEPES, 0.5-MgCl<sub>2</sub>, 1.8-CaCl<sub>2</sub>, and 10-glucose followed by staining with 5  $\mu\text{M}$  Fluo-4 AM ester (Invitrogen, MA, USA) with 0.02% (w/v) Pluronic F-127 (Invitrogen, MA, USA) for calcium imaging or FluoVolt and PowerLoad Concentrate (Invitrogen, MA, USA) for optical action potential measurements for 15–30 min. Prior to imaging, cells were washed twice and imaged in fresh Tyrode's solution using a Nikon Eclipse Ti light microscope<sup>64</sup>. During imaging cells were maintained at 37°C and 5%  $\text{CO}_2$ . Cells were paced at 0–2 Hz with a pulse length of 9 ms and field potential of 23 V using an IonOptix MyoPacer EP field stimulator (IonOptix, MA, USA)<sup>64</sup>. Obtained fluorescence traces underwent background fluorescence subtraction and were normalized as  $\Delta F/F_0$ , where  $\Delta F = F - F_0$ , F is observed fluorescence, and  $F_0$  corresponds to baseline fluorescence. Asymmetric least squares smoothing and the rollingball algorithm with R were used to correct for photobleaching and baseline drift<sup>69,70</sup>. Calcium transients and action potential traces were analyzed using Lab Chart 7 (v7.3.8; AD instruments, CO, USA)<sup>71</sup>.

### Doxorubicin toxicity

iPS cell-derived cardiomyocytes were plated into a 96-well plate 30 days after differentiation. Following ~24 h culture with 0  $\mu\text{M}$ , 0.1  $\mu\text{M}$ , 1  $\mu\text{M}$ , 10  $\mu\text{M}$ , or 20  $\mu\text{M}$  doxorubicin hydrochloride (Sigma Aldrich D1515) in DMSO, cells were stained with a propidium iodide (Invitrogen, MA, USA). Cell counting was conducted using a Cytation 5 cell imaging multimode reader (BioTek, VT, USA) with Gen5 software (BioTek, VT, USA). The impact of doxorubicin on calcium transients was assessed using Fluo-4 (see Fluorescence-based Live Cell Imaging).

### Statistical analysis

Statistics were conducted in R (V.4.2.2). Data was assessed for normality with a Wilk-Shapiro test. Homogeneity of variance for normally distributed data was assessed using an F-test. For nonparametric data, comparisons were made with a Mann-Whitney test. Normally distributed data were compared with a Student's *t*-test if variances were equal or Welch's *t*-test if variances were unequal. A Benjamini-Hochberg correction was employed to control the false discovery rate (FDR) with multiple comparisons. Outliers were defined as values outside 1.5 times the interquartile range for each group. Mean and standard error of the mean are reported unless noted otherwise.

### Data availability

The data that support the findings of this study are available on request from the corresponding author, [A.B.].

Received: 20 November 2024; Accepted: 7 April 2025

Published online: 24 April 2025

### References

1. Takahashi, K. & Yamanaka, S. Induction of pluripotent stem cells from mouse embryonic and adult fibroblast cultures by defined factors. *Cell* **126**, 663–676. <https://doi.org/10.1016/j.cell.2006.07.024> (2006).

2. Behfar, A. et al. Administration of allogenic stem cells dosed to secure cardiogenesis and sustained infarct repair. *Ann. N. Y. Acad. Sci.* **1049**, 189–198. <https://doi.org/10.1196/annals.1334.018> (2005).
3. Behfar, A. et al. Cardiopoietic programming of embryonic stem cells for tumor-free heart repair. *J. Exp. Med.* **204**, 405–420. <https://doi.org/10.1084/jem.20061916> (2007).
4. Nelson, T. J., Martinez-Fernandez, A. & Terzic, A. Induced pluripotent stem cells: Developmental biology to regenerative medicine. *Nat. Rev. Cardiol.* **7**, 700–710. <https://doi.org/10.1038/nrcardio.2010.159> (2010).
5. Musunuru, K. et al. Induced Pluripotent Stem Cells for Cardiovascular Disease Modeling and Precision Medicine: A Scientific Statement From the American Heart Association. *Circ. Genom. Precis. Med.* **11**, e000043. <https://doi.org/10.1161/HCG.0000000000000043> (2018).
6. Arrell, D. K., Niederländer, N. J., Faustino, R. S., Behfar, A. & Terzic, A. Cardioinductive network guiding stem cell differentiation revealed by proteomic cartography of tumor necrosis factor alpha-primed endodermal secretome. *Stem. Cells* **26**, 387–400. <https://doi.org/10.1634/stemcells.2007-0599> (2008).
7. Perez-Terzic, C. et al. Stem cells transform into a cardiac phenotype with remodeling of the nuclear transport machinery. *Nat. Clin. Pract. Cardiovasc. Med.* **4**(Suppl 1), S68–76. <https://doi.org/10.1038/ncpcardio0763> (2007).
8. Zeineddine, D. et al. Oct-3/4 dose dependently regulates specification of embryonic stem cells toward a cardiac lineage and early heart development. *Dev. Cell* **11**, 535–546. <https://doi.org/10.1016/j.devcel.2006.07.013> (2006).
9. Beqqali, A., Kloots, J., Ward-van Oostwaard, D., Mummery, C. & Passier, R. Genome-wide transcriptional profiling of human embryonic stem cells differentiating to cardiomyocytes. *Stem. Cells* **24**, 1956–1967. <https://doi.org/10.1634/stemcells.2006-0054> (2006).
10. Mummery, C. et al. Differentiation of human embryonic stem cells to cardiomyocytes: Role of coculture with visceral endoderm-like cells. *Circulation* **107**, 2733–2740. <https://doi.org/10.1161/01.CIR.0000068356.38592.68> (2003).
11. Mummery, C. L. et al. Differentiation of human embryonic stem cells and induced pluripotent stem cells to cardiomyocytes: a methods overview. *Circ. Res.* **111**, 344–358. <https://doi.org/10.1161/CIRCRESAHA.110.227512> (2012).
12. Laflamme, M. A. et al. Cardiomyocytes derived from human embryonic stem cells in pro-survival factors enhance function of infarcted rat hearts. *Nat. Biotechnol.* **25**, 1015–1024. <https://doi.org/10.1038/nbt1327> (2007).
13. Ueno, S. et al. Biphasic role for Wnt/beta-catenin signaling in cardiac specification in zebrafish and embryonic stem cells. *Proc. Natl. Acad. Sci. U S A* **104**, 9685–9690. <https://doi.org/10.1073/pnas.0702859104> (2007).
14. Lian, X. et al. Directed cardiomyocyte differentiation from human pluripotent stem cells by modulating Wnt/beta-catenin signaling under fully defined conditions. *Nat. Protoc.* **8**, 162–175. <https://doi.org/10.1038/nprot.2012.150> (2013).
15. Lian, X. et al. Robust cardiomyocyte differentiation from human pluripotent stem cells via temporal modulation of canonical Wnt signaling. *Proc. Natl. Acad. Sci. U S A* **109**, E1848–E1857. <https://doi.org/10.1073/pnas.1200250109> (2012).
16. Karbassi, E. et al. Cardiomyocyte maturation: Advances in knowledge and implications for regenerative medicine. *Nat. Rev. Cardiol.* **17**, 341–359. <https://doi.org/10.1038/s41569-019-0331-x> (2020).
17. Kargaran, P. K. et al. Mitochondrial DNA: Hotspot for Potential Gene Modifiers Regulating Hypertrophic Cardiomyopathy. *J. Clin. Med.* <https://doi.org/10.3390/jcm9082349> (2020).
18. Kargaran, P. K., Mosqueira, D. & Kozicz, T. Mitochondrial Medicine: Genetic Underpinnings and Disease Modeling Using Induced Pluripotent Stem Cell Technology. *Front. Cardiovasc. Med.* **7**, 604581. <https://doi.org/10.3389/fcvm.2020.604581> (2020).
19. Takasuna, K., Kazusa, K. & Hayakawa, T. Comprehensive Cardiac Safety Assessment using hiPS-cardiomyocytes (Consortium for Safety Assessment using Human iPS Cells: CSAHi). *Curr. Pharm. Biotechnol.* **21**, 829–841. <https://doi.org/10.2174/1389201020666191024172425> (2020).
20. Guo, Y. & Pu, W. T. Cardiomyocyte Maturation: New Phase in Development. *Circ. Res.* **126**, 1086–1106. <https://doi.org/10.1161/CIRCRESAHA.119.315862> (2020).
21. Yu, L. et al. Molecular and functional changes in voltage-gated Na(+) channels in cardiomyocytes during mouse embryogenesis. *Circ. J.* **75**, 2071–2079. <https://doi.org/10.1253/circj.10-1212> (2011).
22. Hwang, H. S. et al. Comparable calcium handling of human iPSC-derived cardiomyocytes generated by multiple laboratories. *J. Mol. Cell. Cardiol.* **85**, 79–88. <https://doi.org/10.1016/j.yjmcc.2015.05.003> (2015).
23. Huang, C. Y. et al. Enhancement of human iPSC-derived cardiomyocyte maturation by chemical conditioning in a 3D environment. *J. Mol. Cell. Cardiol.* **138**, 1–11. <https://doi.org/10.1016/j.yjmcc.2019.10.001> (2020).
24. Zuppinger, C. 3D Cardiac Cell Culture: A Critical Review of Current Technologies and Applications. *Front. Cardiovasc. Med.* **6**, 87. <https://doi.org/10.3389/fcvm.2019.00087> (2019).
25. Branco, M. A. et al. Transcriptomic analysis of 3D Cardiac Differentiation of Human Induced Pluripotent Stem Cells Reveals Faster Cardiomyocyte Maturation Compared to 2D Culture. *Sci. Rep.* **9**, 9229. <https://doi.org/10.1038/s41598-019-45047-9> (2019).
26. Li, M. et al. Brachyury engineers cardiac repair competent stem cells. *Stem. Cells Transl. Med.* **10**, 385–397. <https://doi.org/10.1002/sctm.20-0193> (2021).
27. Liu, Q. et al. Disruption of mesoderm formation during cardiac differentiation due to developmental exposure to 13-cis-retinoic acid. *Sci. Rep.* **8**, 12960. <https://doi.org/10.1038/s41598-018-31192-0> (2018).
28. Heidi Au, H. T., Cui, B., Chu, Z. E., Veres, T. & Radisic, M. Cell culture chips for simultaneous application of topographical and electrical cues enhance phenotype of cardiomyocytes. *Lab Chip* **9**, 564–575. <https://doi.org/10.1039/b810034a> (2009).
29. Ergir, E. et al. Generation and maturation of human iPSC-derived 3D organotypic cardiac microtissues in long-term culture. *Sci. Rep.* **12**, 17409. <https://doi.org/10.1038/s41598-022-22225-w> (2022).
30. Yang, X. et al. Tri-iodo-L-thyronine promotes the maturation of human cardiomyocytes-derived from induced pluripotent stem cells. *J. Mol. Cell. Cardiol.* **72**, 296–304. <https://doi.org/10.1016/j.yjmcc.2014.04.005> (2014).
31. Yang, X. et al. Fatty Acids Enhance the Maturation of Cardiomyocytes Derived from Human Pluripotent Stem Cells. *Stem Cell Rep.* **13**, 657–668. <https://doi.org/10.1016/j.stemcr.2019.08.013> (2019).
32. Kamakura, T. et al. Ultrastructural maturation of human-induced pluripotent stem cell-derived cardiomyocytes in a long-term culture. *Circ. J.* **77**, 1307–1314. <https://doi.org/10.1253/circj.12-0987> (2013).
33. Yamada, S., Jeon, R., Garmany, A., Behfar, A. & Terzic, A. Screening for regenerative therapy responders in heart failure. *Biomark. Med.* **15**, 775–783. <https://doi.org/10.2217/bmm-2020-0683> (2021).
34. Leonard, A. et al. Afterload promotes maturation of human induced pluripotent stem cell derived cardiomyocytes in engineered heart tissues. *J. Mol. Cell. Cardiol.* **118**, 147–158. <https://doi.org/10.1016/j.yjmcc.2018.03.016> (2018).
35. Li, M. et al. Brachyury engineers cardiac repair competent stem cells. *Stem Cells Transl. Med.* <https://doi.org/10.1002/sctm.20-0193> (2020).
36. Nelson, T. J. et al. CXCR4+/FLK-1+ biomarkers select a cardiopoietic lineage from embryonic stem cells. *Stem Cells* **26**, 1464–1473. <https://doi.org/10.1634/stemcells.2007-0808> (2008).
37. Le, M. N. T., Takahi, M. & Ohnuma, K. Auto/paracrine factors and early Wnt inhibition promote cardiomyocyte differentiation from human induced pluripotent stem cells at initial low cell density. *Sci. Rep.* **11**, 21426. <https://doi.org/10.1038/s41598-021-00763-z> (2021).
38. Zwi, L. et al. Cardiomyocyte differentiation of human induced pluripotent stem cells. *Circulation* **120**, 1513–1523. <https://doi.org/10.1161/CIRCULATIONAHA.109.868885> (2009).
39. Olson, E. N. Gene regulatory networks in the evolution and development of the heart. *Science* **313**, 1922–1927. <https://doi.org/10.1126/science.1132292> (2006).

40. Sheikh, F., Lyon, R. C. & Chen, J. Functions of myosin light chain-2 (MYL2) in cardiac muscle and disease. *Gene* **569**, 14–20. <https://doi.org/10.1016/j.gene.2015.06.027> (2015).
41. Cyganek, L. et al. Deep phenotyping of human induced pluripotent stem cell-derived atrial and ventricular cardiomyocytes. *JCI Insight* <https://doi.org/10.1172/jci.insight.99941> (2018).
42. Shadrin, I. Y. et al. Cardiopatch platform enables maturation and scale-up of human pluripotent stem cell-derived engineered heart tissues. *Nat. Commun.* **8**, 1825. <https://doi.org/10.1038/s41467-017-01946-x> (2017).
43. Ronaldson-Bouchard, K. et al. Advanced maturation of human cardiac tissue grown from pluripotent stem cells. *Nature* **556**, 239–243. <https://doi.org/10.1038/s41586-018-0016-3> (2018).
44. Miki, K. et al. ERRgamma enhances cardiac maturation with T-tubule formation in human iPSC-derived cardiomyocytes. *Nat. Commun.* **12**, 3596. <https://doi.org/10.1038/s41467-021-23816-3> (2021).
45. Fernandez-Ruiz, I. Metabolic reprogramming unlocks the regenerative potential of the heart. *Nat. Rev. Cardiol.* **20**, 795. <https://doi.org/10.1038/s41569-023-00945-4> (2023).
46. Mills, R. J. et al. Functional screening in human cardiac organoids reveals a metabolic mechanism for cardiomyocyte cell cycle arrest. *Proc. Natl. Acad. Sci. U S A* **114**, E8372–E8381. <https://doi.org/10.1073/pnas.1707316114> (2017).
47. Correia, C. et al. Distinct carbon sources affect structural and functional maturation of cardiomyocytes derived from human pluripotent stem cells. *Sci. Rep.* **7**, 8590. <https://doi.org/10.1038/s41598-017-08713-4> (2017).
48. Hu, D. T. et al. Metabolic Maturation of Human Pluripotent Stem Cell-Derived Cardiomyocytes by Inhibition of HIF1alpha and LDHA. *Circ. Res.* **123**, 1066–1079. <https://doi.org/10.1161/CIRCRESAHA.118.313249> (2018).
49. Funakoshi, S. et al. Generation of mature compact ventricular cardiomyocytes from human pluripotent stem cells. *Nat. Commun.* **12**, 3155. <https://doi.org/10.1038/s41467-021-23329-z> (2021).
50. Du, D. T., Hellen, N., Kane, C. & Terracciano, C. M. Action potential morphology of human induced pluripotent stem cell-derived cardiomyocytes does not predict cardiac chamber specificity and is dependent on cell density. *Biophys. J.* **108**, 1–4. <https://doi.org/10.1016/j.bpj.2014.11.008> (2015).
51. Kane, C., Du, D. T., Hellen, N. & Terracciano, C. M. The Fallacy of Assigning Chamber Specificity to iPSC Cardiac Myocytes from Action Potential Morphology. *Biophys. J.* **110**, 281–283. <https://doi.org/10.1016/j.bpj.2015.08.052> (2016).
52. Peinkofer, G. et al. From Early Embryonic to Adult Stage: Comparative Study of Action Potentials of Native and Pluripotent Stem Cell-Derived Cardiomyocytes. *Stem Cells Dev.* **25**, 1397–1406. <https://doi.org/10.1089/scd.2016.0073> (2016).
53. Seibert, F. et al. Electrophysiological and calcium-handling development during long-term culture of human-induced pluripotent stem cell-derived cardiomyocytes. *Basic Res. Cardiol.* **118**, 14. <https://doi.org/10.1007/s00395-022-00973-0> (2023).
54. Liang, P. et al. Drug screening using a library of human induced pluripotent stem cell-derived cardiomyocytes reveals disease-specific patterns of cardiotoxicity. *Circulation* **127**, 1677–1691. <https://doi.org/10.1161/CIRCULATIONAHA.113.001883> (2013).
55. Kostina, A. et al. ER stress and lipid imbalance drive diabetic embryonic cardiomyopathy in an organoid model of human heart development. *Stem Cell Rep.* **19**, 317–330. <https://doi.org/10.1016/j.stemcr.2024.01.003> (2024).
56. Giacomelli, E. et al. Human-iPSC-Derived Cardiac Stromal Cells Enhance Maturation in 3D Cardiac Microtissues and Reveal Non-cardiomyocyte Contributions to Heart Disease. *Cell Stem Cell* **26**(862–879), e811. <https://doi.org/10.1016/j.stem.2020.05.004> (2020).
57. Guo, Z. & Javaheri, A. INKING the Cardiotoxicity Out of Doxorubicin. *JACC Basic Transl. Sci.* **8**, 1008–1009. <https://doi.org/10.1016/j.jacbs.2023.05.001> (2023).
58. Sada, M. et al. IFN-gamma-STAT1-ERK Pathway Mediates Protective Effects of Invariant Natural Killer T Cells Against Doxorubicin-Induced Cardiomyocyte Death. *JACC Basic Transl. Sci.* **8**, 992–1007. <https://doi.org/10.1016/j.jacbs.2023.02.014> (2023).
59. Hundley, W. G. et al. Statins and Left Ventricular Ejection Fraction Following Doxorubicin Treatment. *NEJM Evid.* <https://doi.org/10.1056/evidoa2200097> (2022).
60. Zhao, L. & Zhang, B. Doxorubicin induces cardiotoxicity through upregulation of death receptors mediated apoptosis in cardiomyocytes. *Sci. Rep.* **7**, 44735. <https://doi.org/10.1038/srep44735> (2017).
61. Xia, P. et al. Doxorubicin induces cardiomyocyte apoptosis and atrophy through cyclin-dependent kinase 2-mediated activation of forkhead box O1. *J. Biol. Chem.* **295**, 4265–4276. <https://doi.org/10.1074/jbc.RA119.011571> (2020).
62. Christidi, E. & Brunham, L. R. Regulated cell death pathways in doxorubicin-induced cardiotoxicity. *Cell Death Dis.* **12**, 339. <https://doi.org/10.1038/s41419-021-03614-x> (2021).
63. Sag, C. M., Kohler, A. C., Anderson, M. E., Backs, J. & Maier, L. S. CaMKII-dependent SR Ca leak contributes to doxorubicin-induced impaired Ca handling in isolated cardiac myocytes. *J. Mol. Cell Cardiol.* **51**, 749–759. <https://doi.org/10.1016/j.yjmcc.2011.07.016> (2011).
64. Stutzman, M. J. et al. Characterization of N-terminal RYR2 variants outside CPVT1 hotspot regions using patient iPSCs reveal pathogenesis and therapeutic potential. *Stem Cell Rep.* **17**, 2023–2036. <https://doi.org/10.1016/j.stemcr.2022.07.002> (2022).
65. Livak, K. J. & Schmittgen, T. D. Analysis of relative gene expression data using real-time quantitative PCR and the 2<sup>(-Delta Delta C(T))</sup> Method. *Methods* **25**, 402–408. <https://doi.org/10.1006/meth.2001.1262> (2001).
66. Yuan, J. S., Reed, A., Chen, F. & Stewart, C. N. Jr. Statistical analysis of real-time PCR data. *BMC Bioinform.* **7**, 85. <https://doi.org/10.1186/1471-2105-7-85> (2006).
67. Schindelin, J. et al. Fiji: An open-source platform for biological-image analysis. *Nat. Methods* **9**, 676–682. <https://doi.org/10.1038/nmeth.2019> (2012).
68. Yu, Y. et al. Hepatocyte-like cells differentiated from human induced pluripotent stem cells: Relevance to cellular therapies. *Stem Cell Res.* **9**, 196–207. <https://doi.org/10.1016/j.scr.2012.06.004> (2012).
69. Liland, K. H., Almoy, T. & Mevik, B. H. Optimal choice of baseline correction for multivariate calibration of spectra. *Appl. Spectrosc.* **64**, 1007–1016. <https://doi.org/10.1366/000370210792434350> (2010).
70. Boelens, H. F., Dijkstra, R. J., Eilers, P. H., Fitzpatrick, F. & Westerhuis, J. A. New background correction method for liquid chromatography with diode array detection, infrared spectroscopic detection and Raman spectroscopic detection. *J. Chromatogr. A* **1057**, 21–30. <https://doi.org/10.1016/j.chroma.2004.09.035> (2004).
71. Grune, J. et al. Neutrophils incite and macrophages avert electrical storm after myocardial infarction. *Nat. Cardiovasc. Res.* **1**, 649–664. <https://doi.org/10.1038/s44161-022-00094-w> (2022).

## Acknowledgements

The authors thank Scott Gamb and the Mayo Microscopy and Cell Analysis Core for experimental and technical support. This work was supported by Van Cleve Cardiac Regenerative Program, National Institutes of Health (R01 HL134664), and Marriott Family Foundation. A.G. and R.G. were supported by the National Institute of General Medical Sciences (T32GM145408).

## Author contributions

P.K. and A.G. conception and design, collection and assembly of data, data analysis and interpretation, manuscript writing, final approval of manuscript; R.G., M.J.S., M.S., and C.M.P. collection and assembly of data, final



approval of manuscript; M.J.A. final approval of manuscript; A.T. conception and design, financial and administrative support, final approval of manuscript; A.B. conception and design, financial and administrative support, provision of study material, data interpretation, final approval of manuscript. P.K and A.G. contributed equally.

## Funding

This work was supported by Van Cleve Cardiac Regenerative Program, National Institutes of Health (R01 HL 134664), and Marriott Family Foundation. A.G. and R.G. were supported by the National Institute of General Medical Sciences (T32GM145408).

## Declarations

### Competing interests

A.B., and A.T. are co-inventors on regenerative sciences related intellectual property previously disclosed to Mayo Clinic. Mayo Clinic, A.B., and A.T. have interests in Rion LLC. M.J.A. has received consulting fees from Abbott, BioMarin Pharmaceuticals, Boston Scientific, Bristol-Myers Squibb, Daiichi Sankyo, Illumina, Invitae, Medtronic, Tenaya Therapeutics, and UpToDate; and with Mayo Clinic has license agreements with AliveCor, Anumana, ARMGO Pharma, Pfizer, and Thryv Therapeutics. None of these entities were involved in this study. All other authors have no conflicts of interest to disclose.

### Additional information

**Correspondence** and requests for materials should be addressed to A.B.

**Reprints and permissions information** is available at [www.nature.com/reprints](http://www.nature.com/reprints).

**Publisher's note** Springer Nature remains neutral with regard to jurisdictional claims in published maps and institutional affiliations.

**Open Access** This article is licensed under a Creative Commons Attribution-NonCommercial-NoDerivatives 4.0 International License, which permits any non-commercial use, sharing, distribution and reproduction in any medium or format, as long as you give appropriate credit to the original author(s) and the source, provide a link to the Creative Commons licence, and indicate if you modified the licensed material. You do not have permission under this licence to share adapted material derived from this article or parts of it. The images or other third party material in this article are included in the article's Creative Commons licence, unless indicated otherwise in a credit line to the material. If material is not included in the article's Creative Commons licence and your intended use is not permitted by statutory regulation or exceeds the permitted use, you will need to obtain permission directly from the copyright holder. To view a copy of this licence, visit <http://creativecommons.org/licenses/by-nc-nd/4.0/>.

© The Author(s) 2025